Hole-transport layer-dependent degradation mechanisms in perovskite solar modules: Supplementary Information

Marco Casareto[1, 2], Saivineeth Penukula[2], Wanyi Nie[3], Nicholas Rolston[2]

[1] Materials Science and Engineering, Fulton Schools of Engineering, Arizona State University, Tempe, AZ 85287, USA

[2] Renewable Energy Materials and Devices Lab, School of Electrical, Computer, and Energy Engineering (ECEE), Arizona State University, Tempe, AZ 85281, USA

[3] SUNY University at Buffalo, Department of Physics, Buffalo, NY 14260, USA

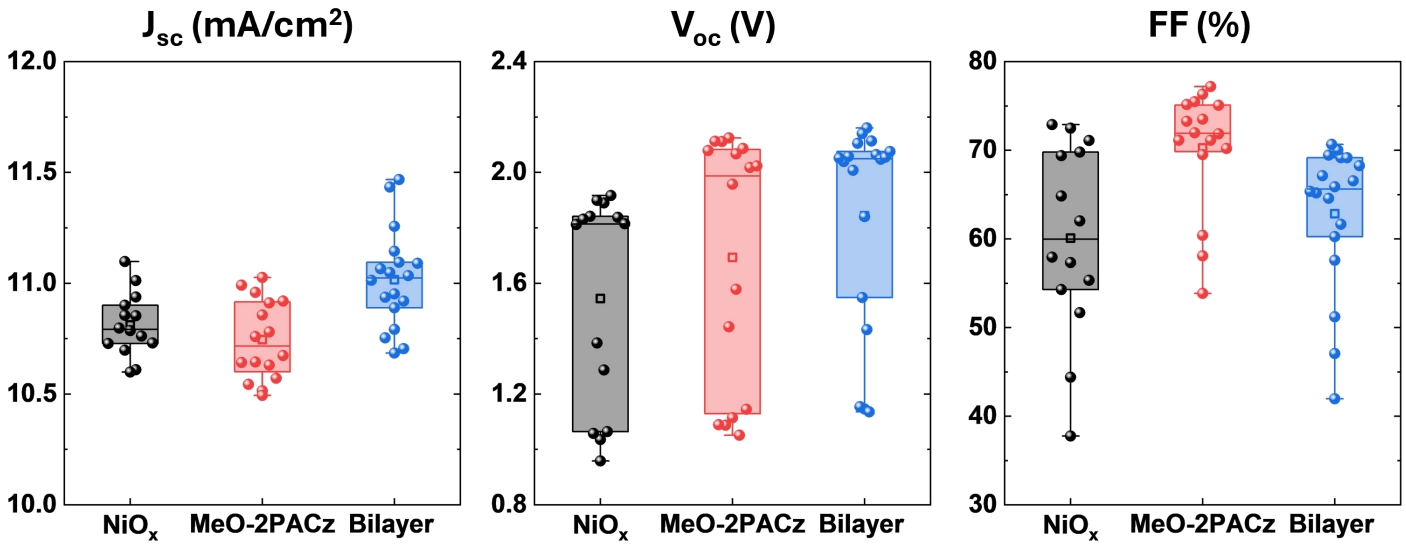

Figure S1: Short-circuit current density (J_{sc}), open-circuit voltage (V_{oc}), and fill factor (FF) of PSMs with differing HTLs after encapsulation.

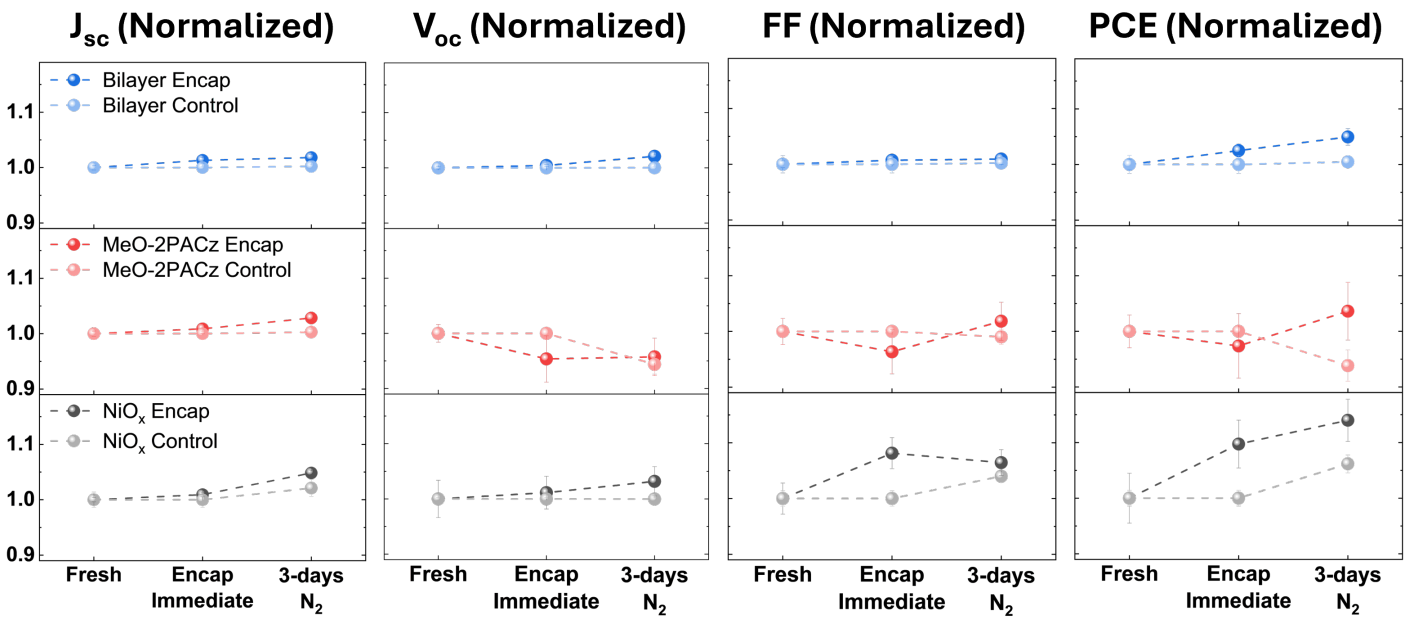

Figure S2: PCE trend of NiO_x (n=30), MeO-2PACz (n=29), and bilayer (n=18) PSCs with encapsulation and time compared to their unencapsulated controls (n=6 for NiO_x and MeO-2PACz, n=5 for bilayer). Values for each sample type are normalized to the mean of the "Fresh" measurements. Unencapsulated controls use the same values for "Encap Immediate" as they do for "Fresh" data points.

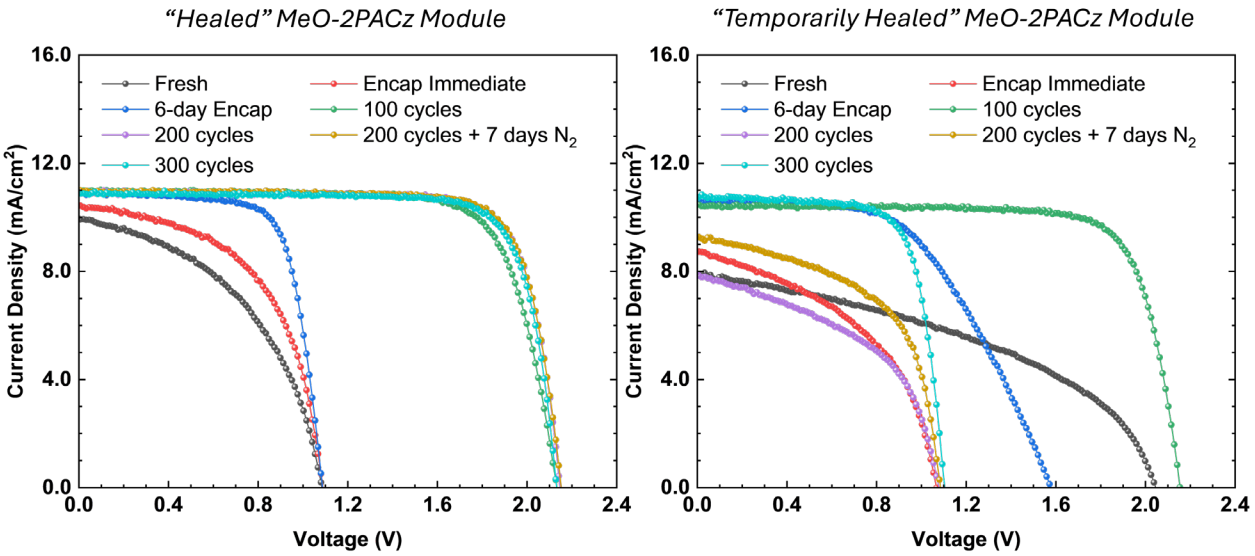

Figure S3: Current-voltage scans of 2 MeO-2PACz PSMs (on different substrates) with encapsulation and cycling. While the "Healed" MeO-2PACz PSM displays immediate improvement in fill factor after encapsulation, the "Temporarily Healed" MeO-2PACz PSM suffers from a significant decrease in V_{oc} immediately after encapsulation that led us to believe a shunt had been introduced from the encapsulation process. The first PSM displays shunt "healing" after 100 cycles, while the second PSM displays a temporary healing after 100 cycles and returns to a shunted behavior for the remaining measurements with cycling.

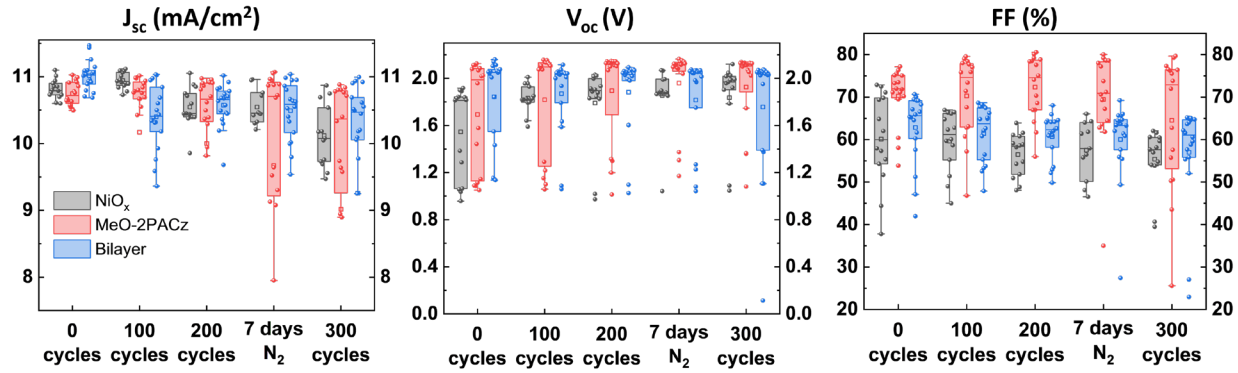

Figure S4: J_{sc}, V_{oc}, and FF trends of PSMs with thermal cycling. Box plots lines indicate 25th, 50th and 75th percentiles, whiskers represent the 5th and 95th percentiles, and a square represents the mean. The vertical scale of the J_{sc} plot excludes several outlier PSMs for MeO-2PACz and bilayer configurations that are in the bottom 5th percentile for their data sets in order to maintain clarity of the plot. Those values are still included in the calculation of the mean and median.

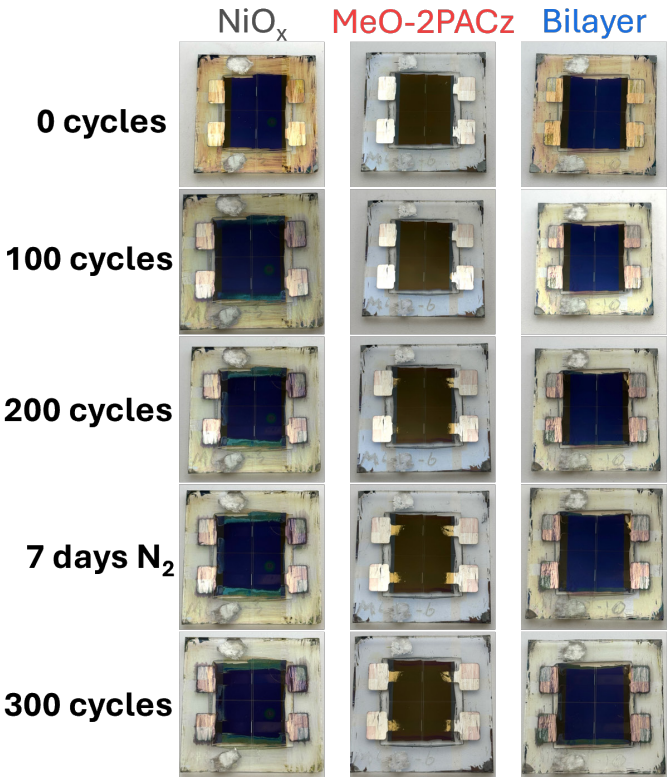

Figure S5: Photographs of representative module substrates for each HTL architecture throughout thermal cycling. The formation of δ-$FAPbI_3$ under the active area of the MeO-2PACz PSMs worsens significantly after 7 days in an N_2 glovebox after 200 thermal cycles.

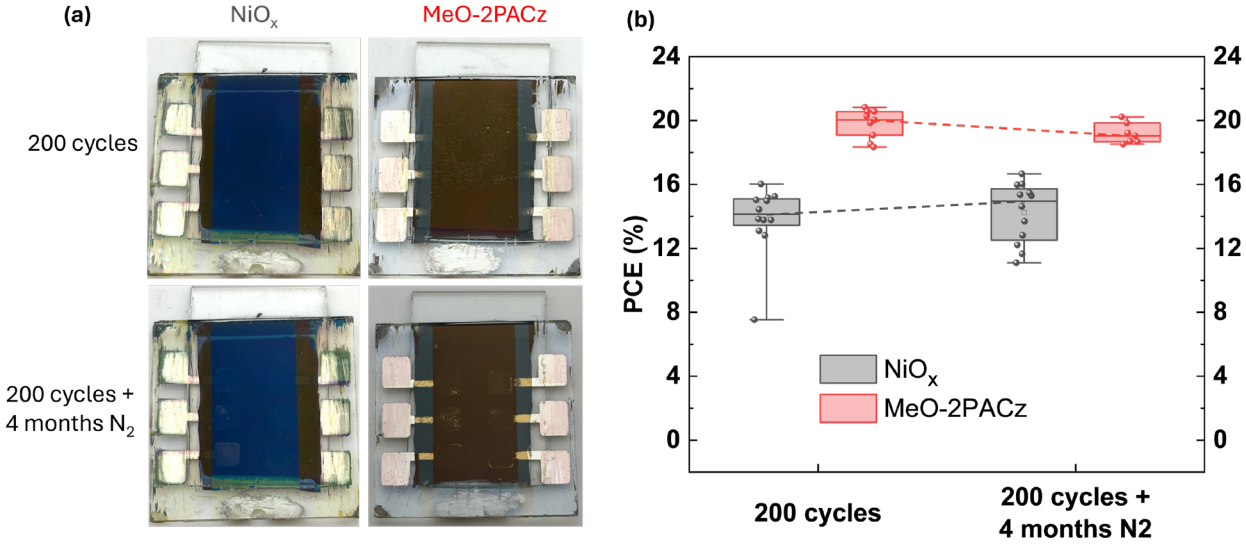

Figure S6: (a) Photographs of NiO_x and MeO-2PACz PSCs immediately after 200 cycles and 4 months after 200 cycles and being stored in the dark in N2 and (b) PCE values of PSCs immediately and 4 months after 200 cycles. 2 pixels on an MeO-2PACz substrate had contact issues during measurements and are excluded from the results. Any pixel that had failed after 200 cycles is excluded to highlight the delayed onset of degradation after cycling.

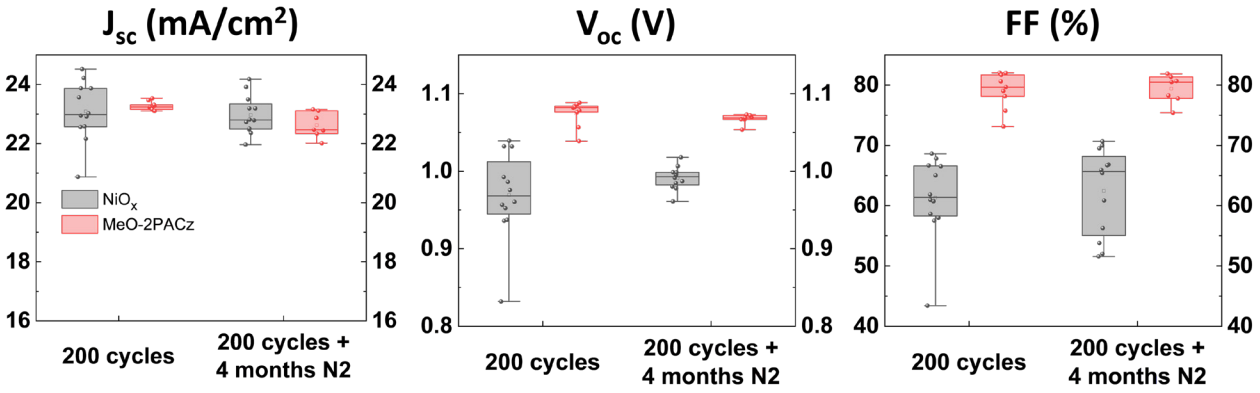

Figure S7: J_{sc}, V_{oc}, and FF of PSCs from Figure S6 after 200 cycles and 4 months later, having been stored in the dark in an N_2 glovebox. Pixels excluded from Figure S6 are also excluded here.

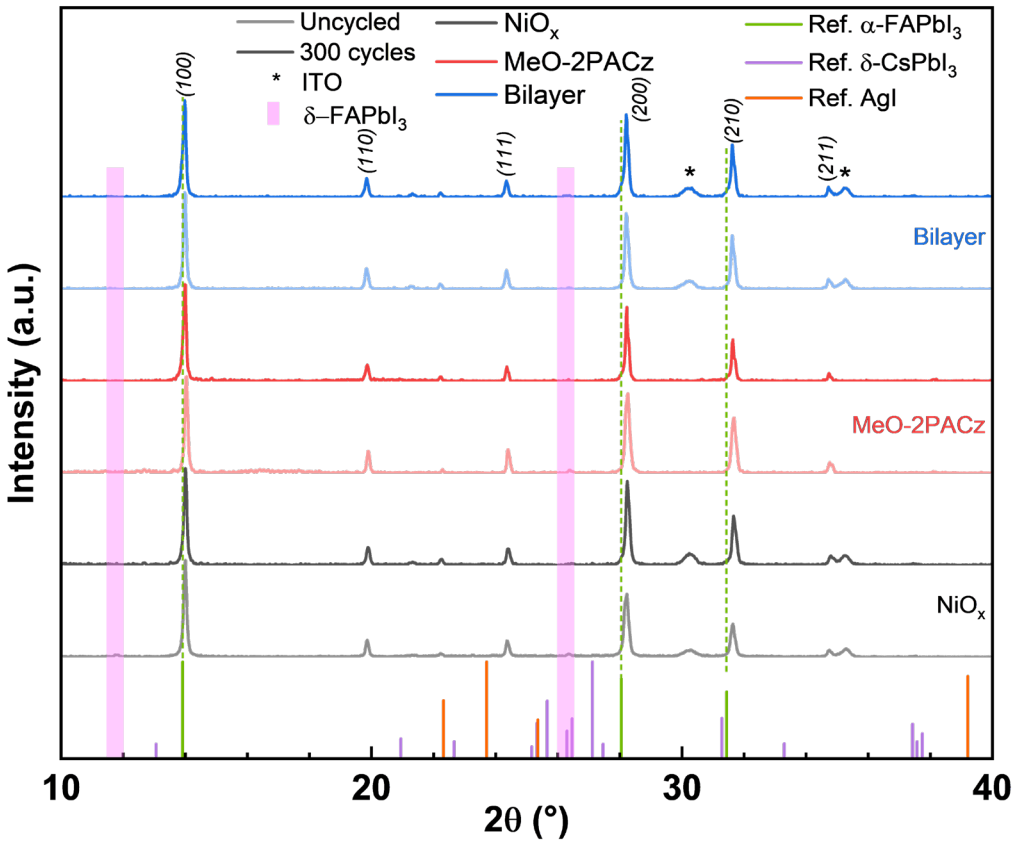

Figure S8: XRD results on the inactive area of uncycled and cycled modules for each HTL architecture. No δ-$FAPbI_3$ is detected for MeO-2PACz PSMs, and the peak shifting/splitting associated with cation phase segregation in NiO_x and bilayer PSMs is not observed.

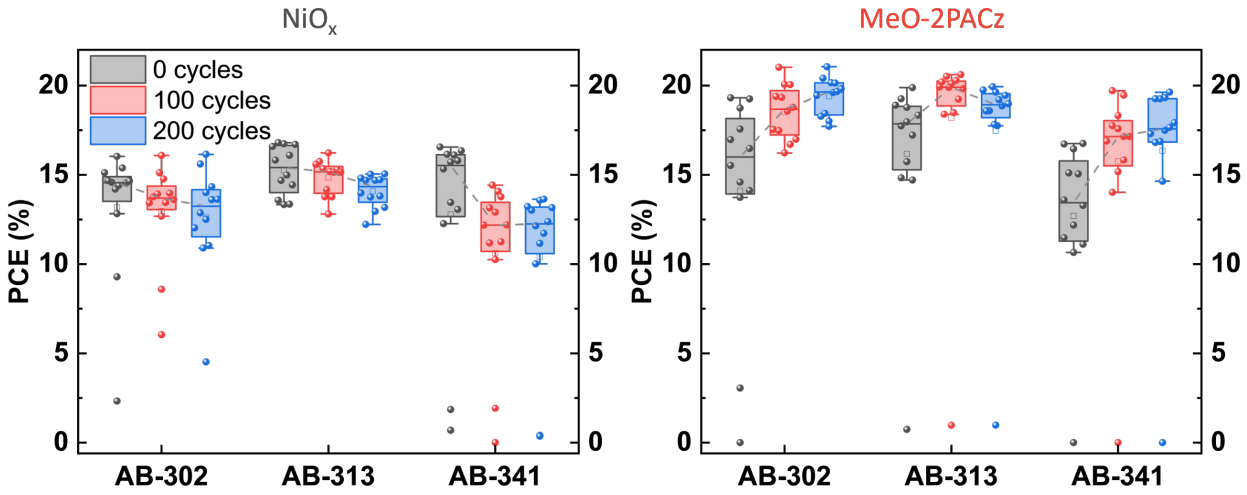

Figure S9: Comparison of the three UV resins used as encapsulants in this study for NiO_x and MeO-2PACz PSCs. While initially there appears to be poorer performance after 100 cycles associated with AB-341 for NiO_x PSCs, this trend was not seen in MeO-2PACz PSCs, leading us to believe systematic error with the encapsulation process owing to the higher viscosity of the AB-341 resin.

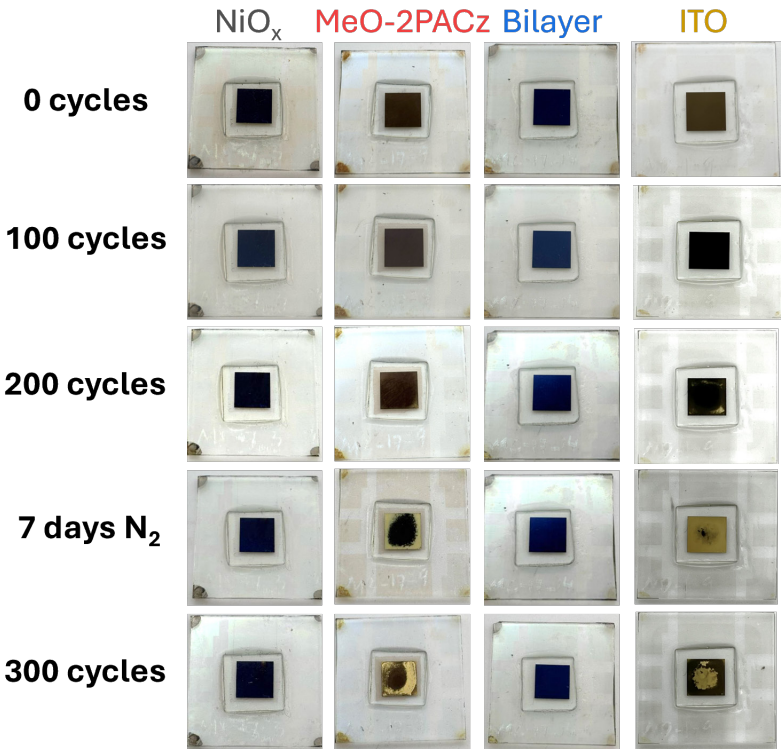

Figure S10: All photographs (uncropped) of test structures encapsulated with AB-302 and a 2.5 mm edge seal width (cropped images of 0, 200, and 7 days N_2 shown in Figure 4). While the discoloration in the ITO sample appears to diminish after 300 cycles, we believe that the degradation may have progressed sufficiently to decompose the C_{60} layer, thus impacting its reflectivity on Ag and the amount of "yellowing" observed.

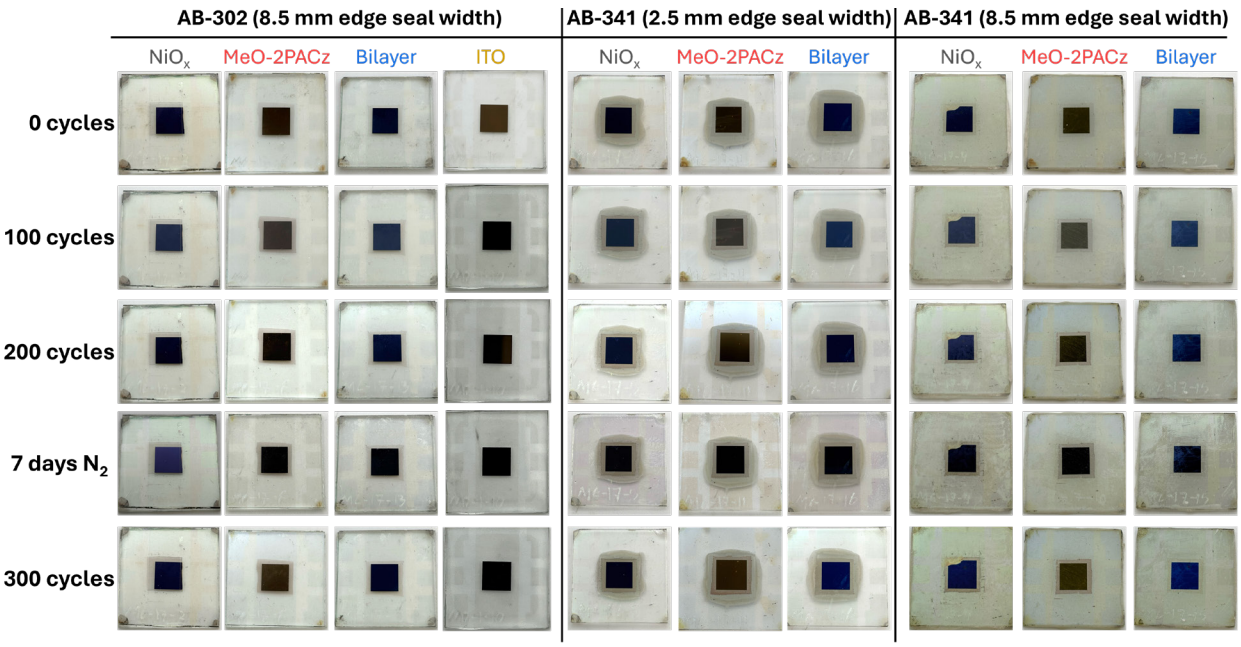

Figure S11: Photographs of remaining test structures to evaluate moisture ingress with thermal cycling. ITO test structures were only encapsulated with AB-302.

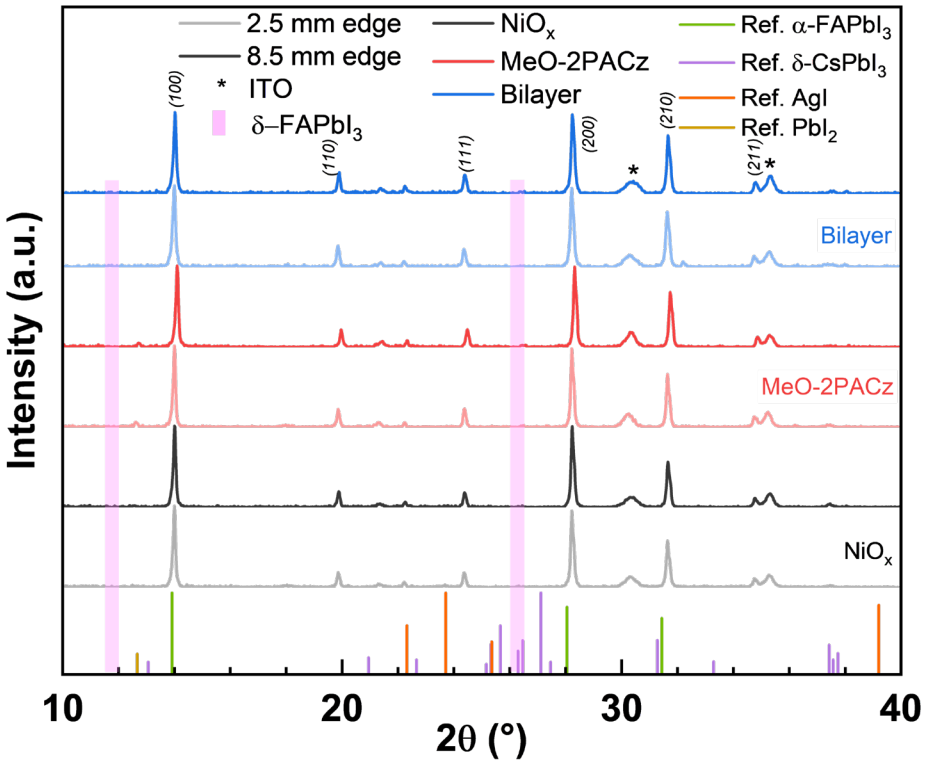

Figure S12: XRD results of test structures encapsulated with Eversolar AB-341 to evaluate moisture and oxygen ingress with thermal cycling. No δ-$FAPbI_3$ or peak splitting associated with cation phase segregation is observed, however a small amount of PbI_2 (2θ =12.67°, ICDD ref. 00-007-0235) forms in the MeO-2PACz structures, indicative of a separate degradation mechanism that does not depend on moisture/oxygen ingress.

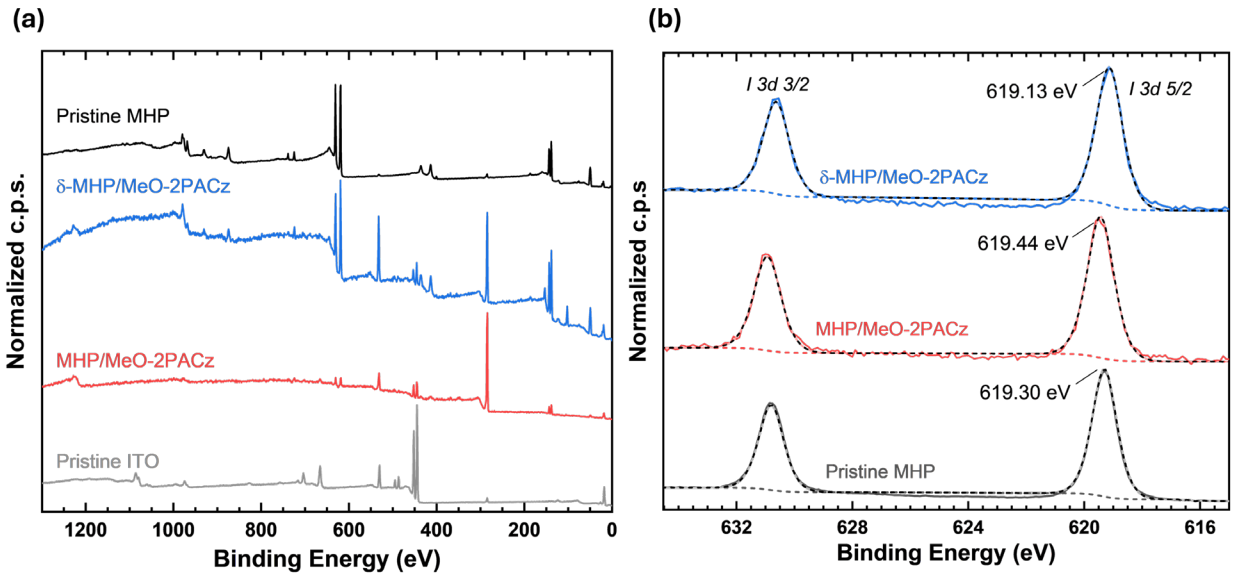

Figure S13: (a) Wide scans for the samples shown in Figure 6 along with pristine MHP. (b) XPS spectra of I 3d peaks for a pristine MHP layer on MeO-2PACz, cycled MHP/MeO-2PACz (no δ-$FAPbI_3$ formation), and cycled δ-MHP/MeO-2PACz (moisture/oxygen ingress, δ-$FAPbI_3$ formation). Peak centers are labeled, and only one synthetic component was used to fit each peak.

Table S1. Binding energy and FWHM of synthetic components for In 3d peak fitting

Sample	**Component**	**3d 5/2 B.E. (eV)**	**FWHM (eV)**
ITO	Screened	444.3 (*444.2±0.4)*	0.85 (*0.9*)
	Unscreened	445.0 (*444.9±0.2)*	1.5 (*1.4*)
MHP/MeO-2PACz	ITO	444.9	0.9
	$In(OH)_3$	445.2 (445.2±0.5)	1.3 (*1.3–1.5*)
	InI_3	446.0 (*445.7±0.6)*	1.1 (*1.0*)
δ-MHP/MeO-2PACz	$In(OH)_3$	445.3	1.0
	InI_3	446.2	1.1

Literature values shown in parentheses, from [1], [2].

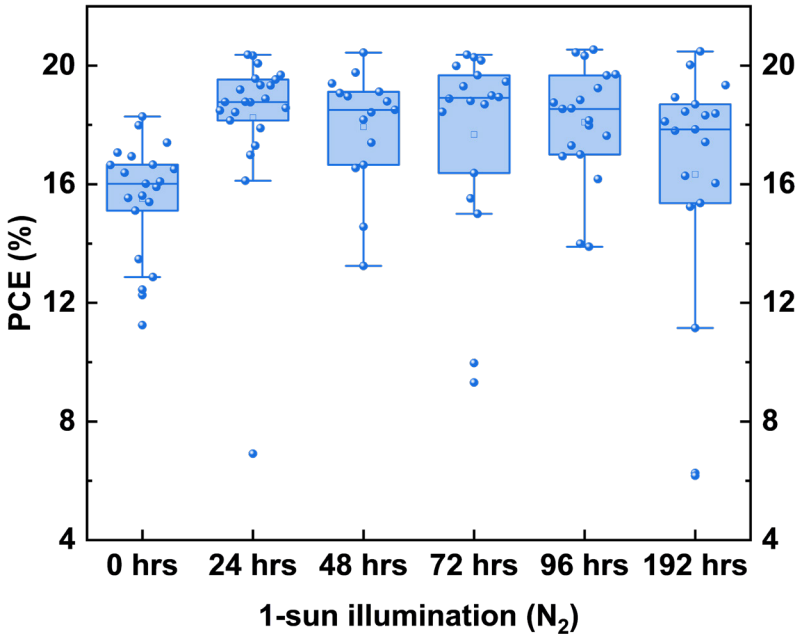

Figure S14: PCE results of bilayer PSCs illuminated in N_2 for ~200 hrs (unmasked).

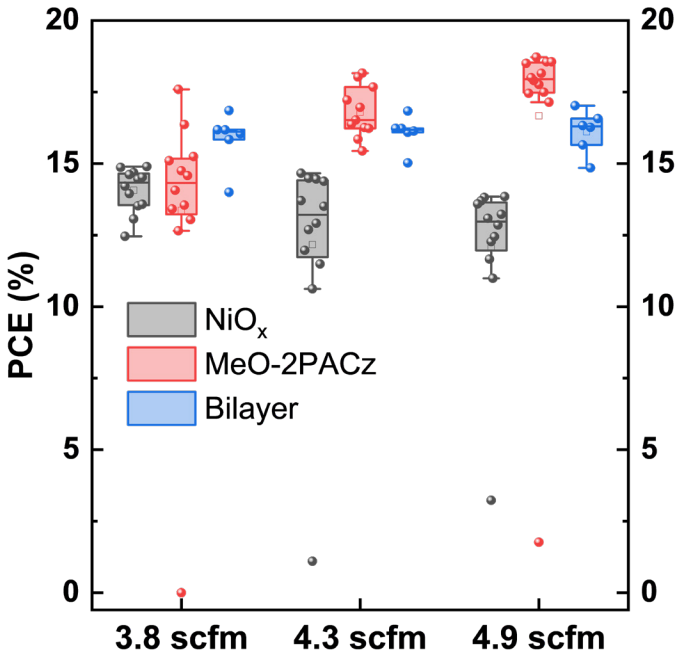

Figure S15: Optimization of flowrates (reported in standard cubic feet/min) for gas quenching of perovskite solar cells on different hole transport layers.

Table S2. Laser scribing parameters for perovskite solar module fabrication

Scribe	Scan Speed (mm/s)	Repetitions	Frequency (kHz)	Raster scan distance (μm) [# lines]	Fluence (mJ/cm^2)
P1 (ITO)	150	5	60	N/A	4.58
P2 (NiO_x/bilayer)	200	1	80	3 [8]	2.55
P2 (MeO-2PACz)	200	3	95	N/A	0.41
P3 (Ag)	200	1	80	3 [8]	2.55

References

[1] G. E. McGUIRE, G. K. Schweitzer, and and A. Thomas Carlson, "Study of Core Electron Binding Energies in Some Group Ilia, Vb, and VIb Compounds 1," 1973. [Online]. Available: https://pubs.acs.org/sharingguidelines

[2] J. D. Henderson, L. Pearson, H. Y. Nie, and M. C. Biesinger, "X-Ray Photoelectron Spectroscopy Analysis of Indium and Indium-Containing Compounds," *Surface and Interface Analysis*, vol. 57, no. 1, pp. 81–97, Jan. 2025, doi: 10.1002/sia.7356.